RESEARCH ARTICLE

Effect of Heteroatom and Charge Reconstruction in Atomically Precise Metal Nanoclusters on Electrochemical Synthesis of Ammonia

Meng Han, Minghao Guo, Yapei Yun, Yujun Xu, Hongting Sheng, Yanxia Chen, Yuanxin Du,* Kun Ni,* Yanwu Zhu, and Manzhou Zhu*

Although atomically precise metal nanoclusters (NCs) are widely used in catalysis, a wide gap exists between state-of-the-art performance and practical requirements. Regulating the intrinsic activity of NCs is critical for the rational design and synthesis of highly efficient catalysts. Herein, M_4Ni_2 NCs (M = Au, Ag) with improved electrocatalytic nitrogen reduction reaction (NRR) activity due to the introduction of Ni are synthesized, which significantly suppresses the H_2 generation competition reaction. Ag_4Ni_2 NCs exhibit the best NRR activity at −0.2 V versus RHE with a NH_3 yield of 23.32 µg mg^{-1} h^{-1} and a faradic efficiency of 78.97% due to the higher N_2 chemisorption ability and lower rate-determining barrier. Meanwhile, ligand partial detachment of NCs during electrocatalysis offers exposed active sites and induces the charge reconstruction, also contributing to the outstanding NRR performance. Based on the precise composition and structure, deep insights into the NRR mechanism at the atom level are provided by in situ Fourier-transformed infrared spectroscopy and ab initial calculation. The study presents an efficient strategy based on heteroatom doping and charges reconstruction to promote NCs catalytic performance.

1. Introduction

Electrocatalytic nitrogen reduction reaction (NRR) can realize the conversion from N_2 to NH_3 at ambient temperature and pressure, which would help reduce the reliance on fossil fuels and greenhouse gas emissions.[1] Although considerable effort has been made in the past few years, the state-of-the-art performance of electrocatalytic NRR is not satisfactory.[2] Atomically precise metal nanoclusters (NCs) have received growing attention as they have performed high activity in catalysis benefiting from the ultra-small size, abundant surface sites, and discrete electronic energy levels.[3] With well-defined composition and structure, NCs provide us the opportunity to identify the active sites and to uncover the catalytic reaction mechanism at the atom level.[4] Although the proceedings, the catalytic activity of most NCs is still far from the requirement of practical applications.[5] Recently, Lu et al. and Yang et al. anchored Au_4Pt_2 and Au_{25} NCs onto defective graphene and S-doped graphene, respectively.[6] In the presence of functional graphene, both the stability and the NRR activity of NCs have been promoted. However, it is greatly desired to improve the intrinsic catalytic activity of NCs by only tuning NCs themselves.

To optimize the catalytic activity, adjusting the inner metal core and outer ligands are two important strategies as they are the major parts of NCs. From the aspect of metal core, a commonly used method is heteroatom doping. In many cases,

M. Han, Y. Yun, H. Sheng, M. Zhu
Department of Chemistry
Anhui University
Hefei 230601, China
E-mail: zmz@ahu.edu.cn
M. Han, Y. Yun, H. Sheng, Y. Du, M. Zhu
Centre for Atomic Engineering of Advanced Materials
Key Laboratory of Structure and Functional Regulation of Hybrid Materials of Ministry of Education
Key Laboratory of Functional Inorganic Material Chemistry of Anhui Province
Anhui University
Hefei 230601, China

M. Guo, K. Ni, Y. Zhu
CAS Key Laboratory of Materials for Energy Conversion
Department of Materials Science and Engineering
iChEM
University of Science and Technology of China
Hefei, Anhui 230026, China
E-mail: nikun@ustc.edu.cn
Y. Xu, Y. Chen
Department of Chemical Physics
University of Science and Technology of China
Hefei 230026, China
Y. Du
Department of Materials Science and Engineering
Anhui University
Hefei 230601, China
E-mail: duyuanxin@ahu.edu.cn

**ADVANCED
SCIENCE NEWS**

www.advancedsciencenews.com

**ADVANCED
FUNCTIONAL
MATERIALS**

www.afm-journal.de

alloyed NCs have shown superior catalytic performances compared with monometallic NCs due to the rational regulation of the composition and electronic structure.[4,7] The type of heteroatom shows a great influence on catalytic activity and selectivity. For instance, Zhu et al. reported that a central single atom doped cluster (M_1Ag_{24}, M = Au, Pd, and Pt) demonstrated completely different catalytic behaviors in the conversion of CO_2 towards C—C bond formation.[8] Lee et al. investigated the effect of metal-doping (M = Au, Pt, and Pd) in M_1Au_{24} and M_2Au_{36} NCs on the electrocatalytic hydrogen evolution reaction (HER) and obtained an activity order of Pt-doped Au NCs>Pd-doped Au NCs>Au NCs.[9] But most of the alloyed NCs have been constructed based on noble metals and their high cost limited practical applications.[6a,9–10] Hence it is essential to bring non-noble metal into NCs catalysts and explore its regulation on catalytic property for considering the cost and practical applications.

Ligands play roles in protecting and stabilizing NCs.[11] However, the overtight and dense cover of ligands would hide the active sites and inhibit the contact between catalyst and reactant.[12] NCs with open structures are highly desired, but it is difficult to obtain NCs with natural open frameworks due to the thermodynamic stability issues.[13] To expose more catalytic active sites, ligand is often removed.[6a,14] Recently, an electrochemical activation has been considered as a facile approach to remove ligand, which not only maintains the stability of NCs but also avoids aggregation, in contrast to the calcination method.[3b,14] Ligand removal has also been speculated to alter the electronic structure and lead to the charge reconstruction of NCs, which however needs further investigations.

Herein, we introduced Ni a poor candidate for HER, to synthesize M_4Ni_2 NCs (M = Au, Ag). The electronic structure of NCs was tuned by heteroatom doping, which suppressed HER and facilitated NRR. The effect of heteroatom species on the catalytic activity and ligand engineering on the charge distribution of NCs were investigated from experimental and computational aspects.

2. Results and Discussion

Taking the advantage of well-defined structures and compositions of atomically precise nanoclusters (NCs), two kinds of NCs ($M_4Ni_2(SR)_8$, M = Au/Ag, SR = 2,4-dimethylthiophenol, M_4Ni_2 for short in the next text) with same crystal structure but different metal occupations have been synthesized to clarify the effect of heteroatom on the electrocatalytic NRR performance. Ag_4Ni_2 NCs were synthesized according to our previous one-pot method.[15] By replacing Ag with Au, Au_4Ni_2 NCs were obtained. The crystal structure of M_4Ni_2 NCs comprises an M_4 unit connecting with two $Ni(SR)_4$ units, as shown in the insets of **Figure 1**a,b, and Table S1 (Supporting Information). The molecular purity of NCs was confirmed by UV–vis absorption spectroscopy and matrix-assisted laser desorption ionization mass spectrometry (MALDI-MS). Ag_4Ni_2 NCs show three fingerprint absorption peaks at 390, 450, and 650 nm,[15] and Au_4Ni_2 NCs exhibit typical characteristic absorption peaks at 380, 457, and 651 nm (Figure 1a,b). In the MALDI-MS spectrum, Ag_4Ni_2 NCs show a molecular ion peak at ≈1646.5 Da, and two fragment peaks at ≈1528 and 1410 Da that are assigned to $Ag_4(SPhMe_2)_8$ and $Ag_2Ni_4(SPhMe_2)_7$, respectively (Figure S1, Supporting
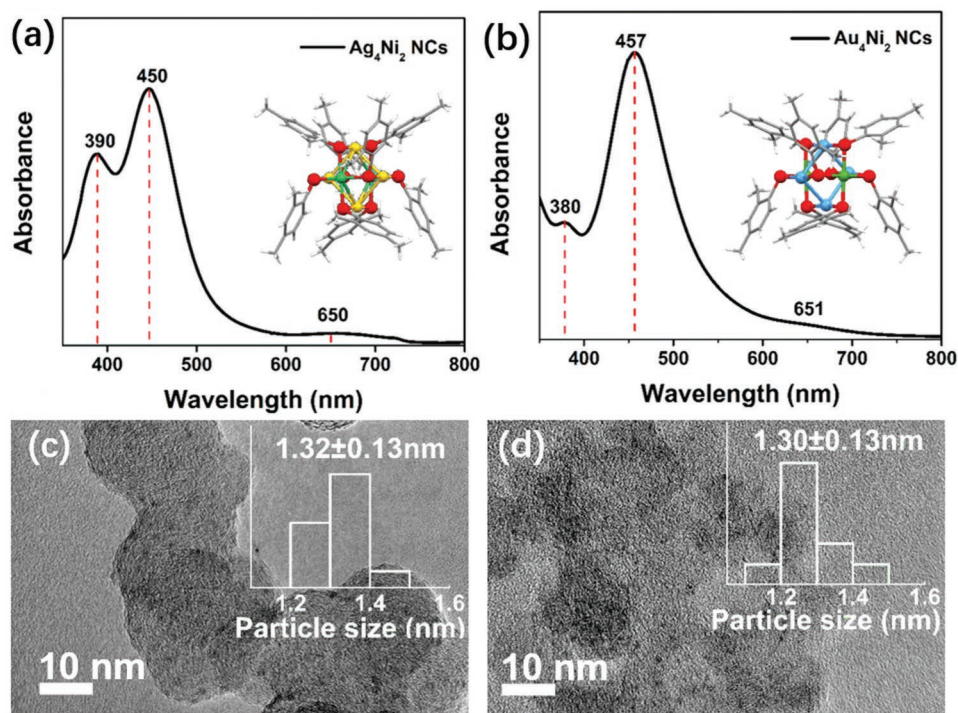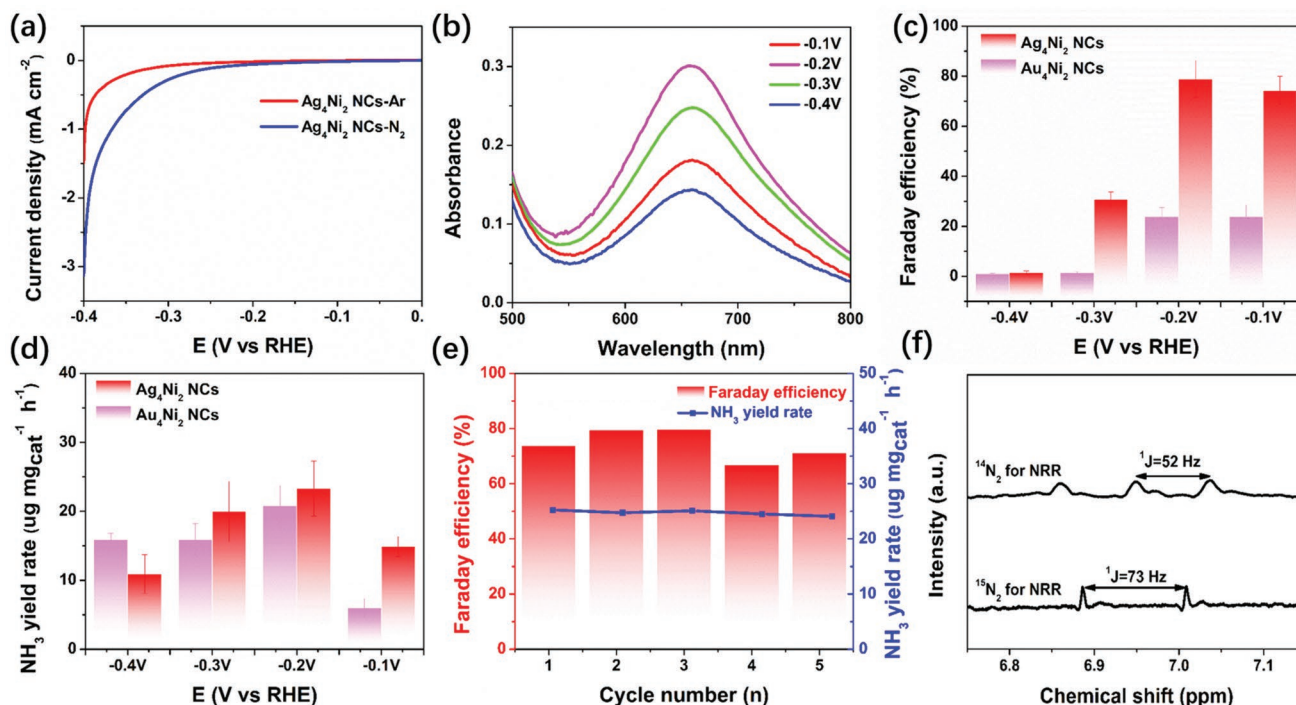

Figure 1. UV–vis absorption spectra of a) Ag_4Ni_2 and b) Au_4Ni_2 NCs in CH_2Cl_2 solution, insets show corresponding crystal structure. HRTEM images and corresponding size distributions of c) Ag_4Ni_2 and d) Au_4Ni_2 NCs loaded on AC. (Color labels: yellow = Ag, blue = Au, red = S, green = Ni, gray = C; White = H).

Information). The peak at 1864.95 Da in the MALDI-MS spectrum of Au_4Ni_2 NCs is assigned to $Au_4Ni_2(SPhMe_2)_7$ (Figure S2, Supporting Information). To evaluate and compare the intrinsic activity of NCs for electrocatalysis, chemically inert activated carbon (AC) was chosen to support the NCs. The successful loading of NCs onto AC was confirmed by high-resolution transmission electron microscope (HRTEM) images (Figure 1c,d). We can see that both NCs are uniformly dispersed on the surface of AC. Statistical analysis shows that the average size of Ag_4Ni_2 or Au_4Ni_2 NCs is 1.32 or 1.30 nm, respectively.

The electrocatalytic NRR performance of NCs was evaluated in 0.1 M HCl solution under ambient conditions by using an H-type cell separated by a Nafion 211 membrane.[16] To probe the initial response of NCs to N_2, linear sweep voltammetry (LSV) tests were first conducted in Ar- or N_2-saturated electrolytes separately. It is worth noting that Ag_4Ni_2 NCs show a more obvious increase in current density in N_2-saturated electrolyte than that in Ar-saturated counterpart, implying Ag_4Ni_2 NCs have a higher NRR activity; the current density of Au_4Ni_2 NCs shows little variation in N_2- or Ar-saturated electrolyte (**Figure 2**a and Figure S3a, Supporting Information). The NH_3 yield rate and Faraday efficiency (FE) of NCs were determined by the chronoamperometry tests. Both types of NCs show stable time-depended current density curves at various potentials (Figures S3b and S4, Supporting Information). After NRR reaction for 4 h, the production of NH_3 and possible by-product N_2H_4 were quantified by UV–vis absorption spectroscopy (Figures S5 and S6, Supporting Information). There is no N_2H_4 detected at all potentials, indicating that N_2 has been completely converted to NH_3 by NCs (Figure S7, Supporting Information). The absorption spectra of the electrolyte stained with the indophenol blue indicator first increase and then decline as the potential becomes negative, and achieves the maximum at −0.2 V, indicating the optimal NRR potential of NCs is −0.2 V (Figure 2b and Figure S3c, Supporting Information). At all potentials, Ag_4Ni_2 NCs exhibit higher FE than that of Au_4Ni_2; the NH_3 yield rate of two types of NCs also displays a similar trend except a reverse occurs at −0.4 V. Ag_4Ni_2 NCs perform the maximum NH_3 yield of 23.32 μg mg_{cat}^{-1} h^{-1} and FE of 78.97% at −0.2, 1.12, and 3.30 V times higher than those of Au_4Ni_2 NCs (NH_3 yield rate: 20.77 μg mg_{cat}^{-1} h^{-1}, FE: 23.92%) (Figure 2c,d). These results suggest that Ag_4Ni_2 NCs have outstanding NRR performance compared with Au_4Ni_2 NCs and other catalysts previously reported (Table S2, Supporting Information).

In order to explore the effect of heteroatom doping on the NRR activity, we synthesized three monometallic NCs with the same number of atoms (M_6 NCs, M = Au, Ag, Ni) as control (Figures S8–S10, Supporting Information). As we can see from Figure 2c,d and Figures S11 and S12 (Supporting Information), both types of M_4Ni_2 NCs display NRR performances superior to M_6 NCs due to the introduction of Ni. Besides, Ag_4Ni_2 NCs inhibit better HER performance than Au_4Ni_2 NCs. The above observations suggest that heteroatom doping plays a vital role in the optimization of the catalytic activity. Moreover, both M_4Ni_2 NCs display almost unchanged current density during the 12 h of NRR evaluation, accompanied by reproducible NH_3 yields and FEs over five consecutive runs at −0.2 V (Figure 2e and Figures S3d and S13, Supporting Information), indicating the excellent durability and recycling. The optical absorption and size distribution of NCs also demonstrate stability (Figure S14

Figure 2. a) LSV curves of Ag_4Ni_2 NCs in Ar- or N_2-saturated electrolyte. b) Indophenol blue reagent chromogenic UV–vis absorption spectra of the products obtained at different potentials catalyzed by Ag_4Ni_2 NCs after reaction for 4 h. c) Average FE and d) NH_3 yield rate of Ag_4Ni_2 and Au_4Ni_2 NCs at different potentials. e) Cycling tests of Ag_4Ni_2 NCs at −0.2 V. f) ^1H NMR spectra of NRR product catalyzed by Ag_4Ni_2 NCs with $^{14}N_2$ or $^{15}N_2$ as feeding gas.

and Figure S15, Supporting Information). To verify the reliability of our experiment results, the control experiments were conducted according to the well-established guideline for detecting interference factors.[17] Under the conditions of N_2-saturated electrolyte at open circuit potential, Ar-saturated electrolyte, and pure AC in N_2-saturated electrolyte −0.2 V, all the absorption spectra corresponding to NH_3 content are extremely close to blank (Figure S16, Supporting Information). Therefore, NH_3 has been produced by N_2 reduction in the presence of a catalyst. Furthermore, in order to confirm the source of nitrogen for NH_3 production, we also conducted isotope labeling experiments. As expected, the obtained product by using $^{14}N_2$ and $^{15}N_2$ as feeding gas appears clear $^{14}NH_4^+$ and $^{15}NH_4^+$ nuclear magnetic resonance (NMR) feature signals, respectively (Figure 2f).[18] These results prove that the N source in NH_3 is from the N_2.

X-ray photoelectron spectroscopy (XPS) was used to analyze the chemical valance state of NCs before and after catalysis. As shown in **Figure 3**a, the Ag 3d spectrum of Ag_4Ni_2 NCs shows two strong peaks at binding energies of 369.41 and 375.44 eV corresponding to Ag $3d_{5/2}$ and Ag $3d_{3/2}$ of Ag(I), and the Ni 2p spectrum shows two peaks at 853.95 and 871.15 eV ascribed to Ni $2p_{3/2}$ and Ni $2p_{1/2}$, indicating that the valence of nickel is +2.[15] The valence states of Au and Ni in Au_4Ni_2 NCs are +1 and +2, respectively (Figure S17, Supporting Information).[19] After NCs are loaded on AC, the chemical environment is maintained. The S/metal ratio determined by XPS is 1.09 or 1.05 for Ag_4Ni_2 NCs or Au_4Ni_2 NCs, respectively. After NRR, the S/metal ratio is 0.6 or 0.8 for Ag_4Ni_2 NCs or Au_4Ni_2 NCs, respectively, which is obviously reduced compared with that before reaction, confirming the partial ligand detachment (Table S3, Supporting Information). Besides, the binding energies of Ag 3d and Au 4f in Ag_4Ni_2 and Au_4Ni_2 NCs show negative and positive shifts, respectively, suggesting the electron density of Ag and Au are reduced. The positive shift of Ni XPS peaks also confirms the decrease of Ni electron density. However, the decline of S 2p binding energies suggests that the electron density of S is increased in both NCs. These results indicate that the electron transfer occurs between metal and S atoms, which may be caused by the charge reconstruction in the cluster due to the ligand removal in the electrocatalytic process.[14] It is worth noting that the interaction between metal and S atoms in Ag_4Ni_2 NCs is greater than that in Au_4Ni_2 NCs, which further indicates that the heteroatom species have an important

influence on the regulation of cluster electronic structure (Figure 3 and Figure S17, Supporting Information).

To insight the reason of the NRR activity difference between Ag_4Ni_2 NCs and Au_4Ni_2 NCs, N_2 temperature-programmed desorption (TPD) experiment was conducted to evaluate the N_2 adsorption capability of NCs. As shown in **Figure 4**a, both NCs have two distinct peaks. The peak in the range of 100–200 °C and 270–400 °C are attributed to the physisorption and chemisorption of N_2, respectively.[20] The TPD signal of Ag_4Ni_2 NCs is significantly higher than that of Au_4Ni_2 NCs, suggesting Ag_4Ni_2 NCs is favorable for N_2 adsorption, thus facilitating NRR.

To further reveal the NRR transformation process on the catalyst surface, in situ Fourier transform infrared (FTIR) spectra of Ag_4Ni_2 NCs were recorded at −0.2 V for 30 min. As shown in Figure 4b, three independent peaks increase with time, confirming that the essential intermediates are generated during the NRR process. The peaks at 1320, 1475, and 1582 cm^{-1} correspond to the $-NH_2-$ wagging, H−N−H bending, and the characteristic absorption of NH_4^+ or NH_3 molecules, respectively.[21] The experimental results provide direct evidence for the formation of $^*N_2H_y$ intermediates ($1 \leq y \leq 4$) (* means the adsorbed species) on the surface of Ag_4Ni_2 NCs, and the detailed reaction pathway is further presented by the combination with the theoretical calculation results as discussed followed.

In order to get deep knowledge of the structural and electronic origin of the NRR activity of Au_4Ni_2 and Ag_4Ni_2 NCs, density functional theory (DFT) simulations were performed. The adsorption energies of N_2 molecules onto the clusters with or without ligands are firstly discussed. For the intact clusters, the physical adsorption of N_2 is weak, e.g., ≈−0.2 to 0.4 eV for Au_4Ni_2 NCs and ≈−0.2 to −0.1 eV for Ag_4Ni_2 NCs, suggesting that the tight coverage of ligands hinders the further NRR reactions (Figure S18 and S19, Supporting Information). Partial ligand removal is beneficial for the exposure of the active sites, and it is worthy to study whether the dethiolated metal site or the dealkylated S site is the catalytic active site. Therefore, we discuss two situations here, $-C_8H_9$ or $-SC_8H_9$ removed from the cluster. The calculated adsorption energy of N_2 on Au_4Ni_2 NCs with the removal of $-C_8H_9$ is ≈−0.1 eV and on Ag_4Ni_2 NCs with the removal of $-C_8H_9$ is ≈−0.2 to −0.1 eV, also demonstrating a weak physical adsorption behavior (Figures S20 and S21, Supporting Information). When considering $-SC_8H_9$ is removed, the calculated adsorption energy is ≈−0.1 to −0.2 eV on Au_4Ni_2 NCs and ≈−0.2 to −0.3 eV on Ag_4Ni_2 NCs, especially
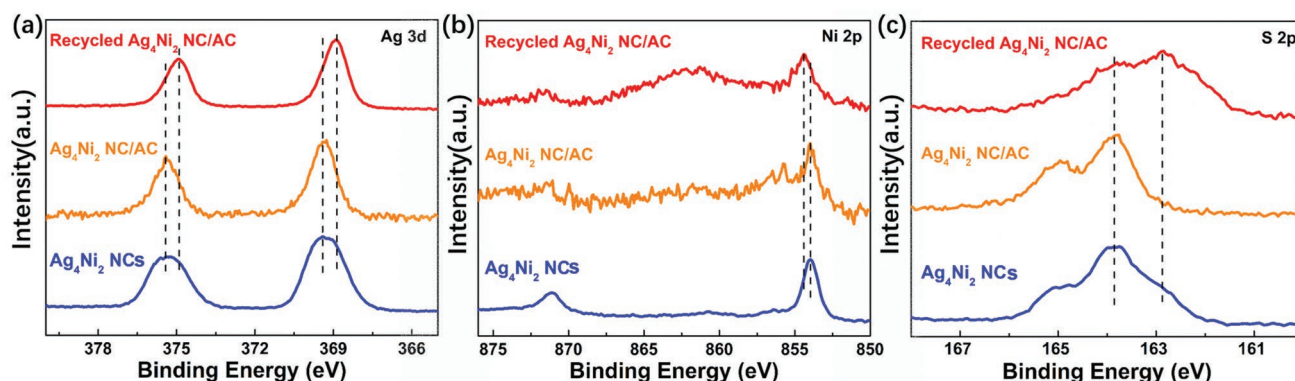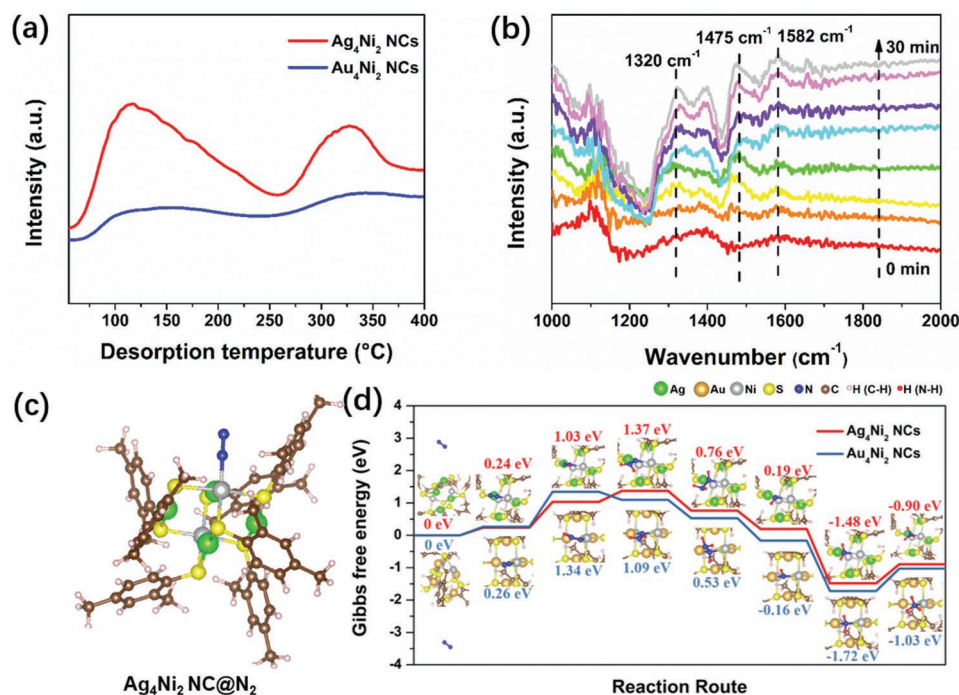

Figure 3. a) Ag 3d, b) Ni 2p, and c) S 2p XPS spectra of Ag_4Ni_2 NCs, and Ag_4Ni_2 NC /AC before and after NRR.

Figure 4. a) N_2-TPD tests of Au_4Ni_2 and Ag_4Ni_2 NCs. b) In situ FTIR spectra of Ag_4Ni_2 NCs at −0.2 V. c) The optimized configuration of Ag_4Ni_2 NCs with N_2 adsorption. d) The Gibbs free energy path of NRR reaction on Ag_4Ni_2 and Au_4Ni_2 NCs.

−0.34 eV on the Ni-site of Ag_4Ni_2 NCs, showing a stronger chemical adsorption behavior and paving the way for further NRR reactions (Figures S22 and S23, Supporting Information). Thus, the dethiolated Ni site is identified as the active site and the models with −SC_8H_9 removal are considered for further NRR reactions, as shown in Figure 4c.

The Gibbs energy diagrams of NRR reactions on Au_4Ni_2 and Ag_4Ni_2 NCs with -SC_8H_9 ligand fall off are shown in Figure 4d. For both NCs, the Gibbs energy of NNH$_2$* state is lower than the NHNH* state, the NHNH$_2$* state is lower than the N* state, the NH* state is lower than the NH$_2$NH$_2$* state, indicating the most possible reaction path is N_2+*→N_2*→NNH*→NNH$_2$*→ NHNH$_2$*→ NH*→ NH$_2$*→NH$_3$*, with the consideration of three possible reaction paths (Figures S24–S26, Supporting Information). Furthermore, Ag_4Ni_2 NCs have a lower Gibbs energy raise of 0.79 eV in the rate-determining step of N_2*→NNH*, comparing to 1.08 eV in Au_4Ni_2 NCs, indicating a higher activity toward NRR of Ag_4Ni_2 NCs.

The electronic origin of the NRR catalytic activity of clusters was discussed by calculating Crystal Orbital Hamiltonian Population Analysis (COHP) and d-band center. When N_2 is adsorbed on Ag_4Ni_2 NCs, the length of N≡N is longer and the distance between N and Ni is shorter in comparison to that adsorbed on Au_4Ni_2 NCs (Figure S27a,b, Supporting Information). Besides, the integral value of COHP (ICOHP) from the deep energy state to Fermi level indicates the strength of the considered interaction between two selected atoms. The ICOHP of N—N interaction of N_2 molecule adsorbed on Ag_4Ni_2 NCs is -21.80 eV, which has a lower absolute value than −21.96 eV on Au_4Ni_2 NCs, indicating the weakened N≡N bond in N_2 molecular on Ag_4Ni_2 NCs (Figure S27c, Supporting Information). In addi-

tion, the ICOHP of N—Ni interaction between N_2 molecular and active Ni site on Ag_4Ni_2 NCs is -4.59 eV, which has a higher absolute value than −4.48 eV on Au_4Ni_2 NCs, showing strengthened adsorption of N_2 on Ag_4Ni_2 NCs (Figure S27d, Supporting Information). Besides, d-band centers of the active Ni site for NCs with or without -SC_8H_9 removal were calculated. For intact NCs, the d-band center of Ag_4Ni_2 NCs is at −1.278 eV, which is deeper than that of Au_4Ni_2 NCs (−1.186 eV), and becomes to be −1.107 eV, which is higher than that of Au_4Ni_2 NCs (−1.130 eV) when the ligand is removed (Figure S28, Supporting Information). Considering higher d-band center benefits N_2 adsorption, the above results suggest that the removal of ligand is of vital importance for the stronger chemical adsorption of N_2 molecule, especially for Ag_4Ni_2 NCs, which is in accordance with the N_2-TPD experimental results.

3. Conclusion

By introducing a poor-HER component Ni, M_4Ni_2 NCs (M = Au, Ag) with superior NRR activity were synthesized, compared with monometallic M_6 NCs (M = Au, Ag, Ni). The effect of heteroatom species on the NRR activity was further investigated. Ag_4Ni_2 NCs showed better catalytic NRR performance than Au_4Ni_2 due to its stronger N_2 chemisorption ability and lower rate-determining barrier. Meanwhile, electrochemical induced ligand partial removal allowed reactant easily contact with catalytic sites as well as resulted in the charge reconstruction, benefiting catalytic activity. NRR reaction pathway and corresponding *N_2H_y intermediates were demonstrated by DFT calculation and in situ FTIR. The promotion of intrinsic

**ADVANCED
SCIENCE NEWS**

www.advancedsciencenews.com

**ADVANCED
FUNCTIONAL
MATERIALS**

www.afm-journal.de

catalytic activity on the basis of heteroatom doping and charge reconstruction can be extended to developing highly efficient catalysts.

Supporting Information

Supporting Information is available from the Wiley Online Library or from the author.

Conflict of Interest

The authors declare no conflict of interest.

Data Availability Statement

The data that support the findings of this study are available in the supplementary material of this article.

[1] a) X. Wang, M. Luo, J. Lan, M. Peng, Y. Tan, *Adv. Mater.* **2021**, *33*, 2007733; b) T. Wu, M. M. Melander, K. Honkala, *ACS Catal.* **2022**, *12*, 2505; c) M. Yuan, J. Chen, Y. Bai, Z. Liu, J. Zhang, T. Zhao, Q. Shi, S. Li, X. Wang, G. Zhang, *Chem. Sci.* **2021**, *12*, 6048; d) M. Yuan, J. Chen, Y. Xu, R. Liu, T. Zhao, J. Zhang, Z. Ren, Z. Liu, C. Streb, H. He, C. Yang, S. Zhang, G. Zhang, *Energy Environ. Sci.* **2021**, *14*, 6605; e) M. Yuan, J. Chen, Y. Bai, Z. Liu, J. Zhang, T. Zhao, Q. Wang, S. Li, H. He, G. Zhang, *Angew. Chem., Int. Ed.* **2021**, *60*, 10910.
[2] Y. Liu, P. Deng, R. Wu, X. Zhang, C. Sun, H. Li, *J. Mater. Chem. A* **2021**, *9*, 6694.
[3] a) X. Cai, W. Hu, S. Xu, D. Yang, M. Chen, M. Shu, R. Si, W. Ding, Y. Zhu, *J. Am. Chem. Soc.* **2020**, *142*, 4141; b) H. Seong, V. Efremov, G. Park, H. Kim, J. S. Yoo, D. Lee, *Angew. Chem., Int. Ed. Engl.* **2021**, *60*, 14563; c) Y. Xiong, H. Chen, S. Yang, X. Xue, L. He, X. Liu, J. Ma, Z. Jin, *Nano Lett.* **2021**, *21*, 8693; d) D. Yang, W. Pei, S. Zhou, J. Zhao, W. Ding, Y. Zhu, *Angew. Chem., Int. Ed. Engl.* **2020**, *59*, 1919.
[4] Y. Du, J. Xiang, K. Ni, Y. Yun, G. Sun, X. Yuan, H. Sheng, Y. Zhu, M. Zhu, *Inorg. Chem. Front.* **2018**, *5*, 2948.
[5] D. R. MacFarlane, P. V. Cherepanov, J. Choi, B. H. R. Suryanto, R. Y. Hodgetts, J. M. Bakker, F. M. Ferrero Vallana, A. N. Simonov, *Joule* **2020**, *4*, 1186.
[6] a) C. Yao, N. Guo, S. Xi, C. Q. Xu, W. Liu, X. Zhao, J. Li, H. Fang, J. Su, Z. Chen, H. Yan, Z. Qiu, P. Lyu, C. Chen, H. Xu, X. Peng, X. Li, B. Liu, C. Su, S. J. Pennycook, C. J. Sun, J. Li, C. Zhang, Y. Du, J. Lu, *Nat. Commun.* **2020**, *11*, 4389; b) M. Li, B. Zhang, T. Cheng, S. Yu, S. Louisia, C. Chen, S. Chen, S. Cestellos-Blanco, W. A. Goddard, P. Yang, *Nano Res.* **2021**, *14*, 3509.
[7] a) H. Qian, D. E. Jiang, G. Li, C. Gayathri, A. Das, R. R. Gil, R. Jin, *J. Am. Chem. Soc.* **2012**, *134*, 16159; b) S. Xie, H. Tsunoyama, W. Kurashige, Y. Negishi, T. Tsukuda, *ACS Catal.* **2012**, *2*, 1519.
[8] Y. Liu, X. Chai, X. Cai, M. Chen, R. Jin, W. Ding, Y. Zhu, *Angew. Chem., Int. Ed. Engl.* **2018**, *57*, 9775.
[9] W. Choi, G. Hu, K. Kwak, M. Kim, D. E. Jiang, J. P. Choi, D. Lee, *ACS Appl. Mater. Interfaces* **2018**, *10*, 44645.
[10] X. Zou, S. He, X. Kang, S. Chen, H. Yu, S. Jin, D. Astruc, M. Zhu, *Chem. Sci.* **2021**, *12*, 3660.
[11] a) X. Wan, J. Wang, Z. Nan, Q. Wang, *Sci. Adv.* **2017**, *3*, e1701823; b) R. R. Nasaruddin, T. Chen, N. Yan, J. Xie, *Coord. Chem. Rev.* **2018**, *368*, 60.
[12] a) M. Turner, V. B. Golovko, O. P. H. Vaughan, P. Abdulkin, A. Berenguer-Murcia, M. S. Tikhov, B. F. G. Johnson, R. M. Lambert, *Nature* **2008**, *454*, 981; b) S. Yamazoe, K. Koyasu, T. Tsukuda, *Acc. Chem. Res.* **2014**, *47*, 816.
[13] a) S. F. Yuan, Z. Lei, Z. J. Guan, Q. M. Wang, *Angew. Chem., Int. Ed. Engl.* **2021**, *60*, 5225; b) Z. Wu, D. R. Mullins, L. F. Allard, Q. Zhang, L. Wang, *Chin. Chem. Lett.* **2018**, *29*, 795.
[14] Y. Sun, X. Liu, K. Xiao, Y. Zhu, M. Chen, *ACS Catal.* **2021**, *11*, 11551.
[15] G. Sun, X. Kang, S. Jin, X. Li, D. Hu, S. Wang, M. Zhu, *Acta Phys.-Chim. Sin.* **2018**, *34*, 799.
[16] M. Yuan, Q. Li, J. Zhang, J. Wu, T. Zhao, Z. Liu, L. Zhou, H. He, B. Li, G. Zhang, *Adv. Funct. Mater.* **2020**, *30*, 2004208.
[17] H.-L. Du, T. R. Gengenbach, R. Hodgetts, D. R. MacFarlane, A. N. Simonov, *ACS Sustainable Chem. Eng.* **2019**, *7*, 6839.
[18] Y. Gu, B. Xi, W. Tian, H. Zhang, Q. Fu, S. Xiong, *Adv. Mater.* **2021**, *33*, 2100429.
[19] B. Wang, Y. Yue, X. Pang, M. Yu, T. Wang, R. Chang, Z. Pan, J. Zhao, X. Li, *J. Catal.* **2021**, *404*, 198.
[20] a) M. Zhang, C. Choi, R. Huo, G. H. Gu, S. Hong, C. Yan, S. Xu, A. W. Robertson, J. Qiu, Y. Jung, Z. Sun, *Nano Energy* **2020**, *68*, 104323; b) Y. Yang, L. Zhang, Z. Hu, Y. Zheng, C. Tang, P. Chen, R. Wang, K. Qiu, J. Mao, T. Ling, S. Z. Qiao, *Angew. Chem., Int. Ed. Engl.* **2020**, *59*, 4525.
[21] a) X. W. Lv, X. L. Liu, Y. J. Suo, Y. P. Liu, Z. Y. Yuan, *ACS Nano* **2021**, *15*, 12109; b) J. Qin, B. Liu, K.-H. Lam, S. Song, X. Li, X. Hu, *ACS Sustainable Chem. Eng.* **2020**, *8*, 17791.